Supplementary Information

Hexagonal Mg$_2$B$_2$ and Ca$_2$B$_2$ monolayers as promising anode materials for Li-ion and Na-ion batteries

Yuqi Sun, Kaiqi Li, Bing Wang, Weiming Zhang, Erpeng Wang, Jian Zhou[*] and

Zhimei Sun[*]

School of Materials Science and Engineering, Beihang University, Beijing 100191, China

*Corresponding authors.

E-mail addresses: jzhou@buaa.edu.cn (J.Zhou), zmsun@buaa.edu.cn (Z. Sun)

# 1. Dynamic stabilities of bulk MB$_2$ and M$_2$B$_2$ monolayers
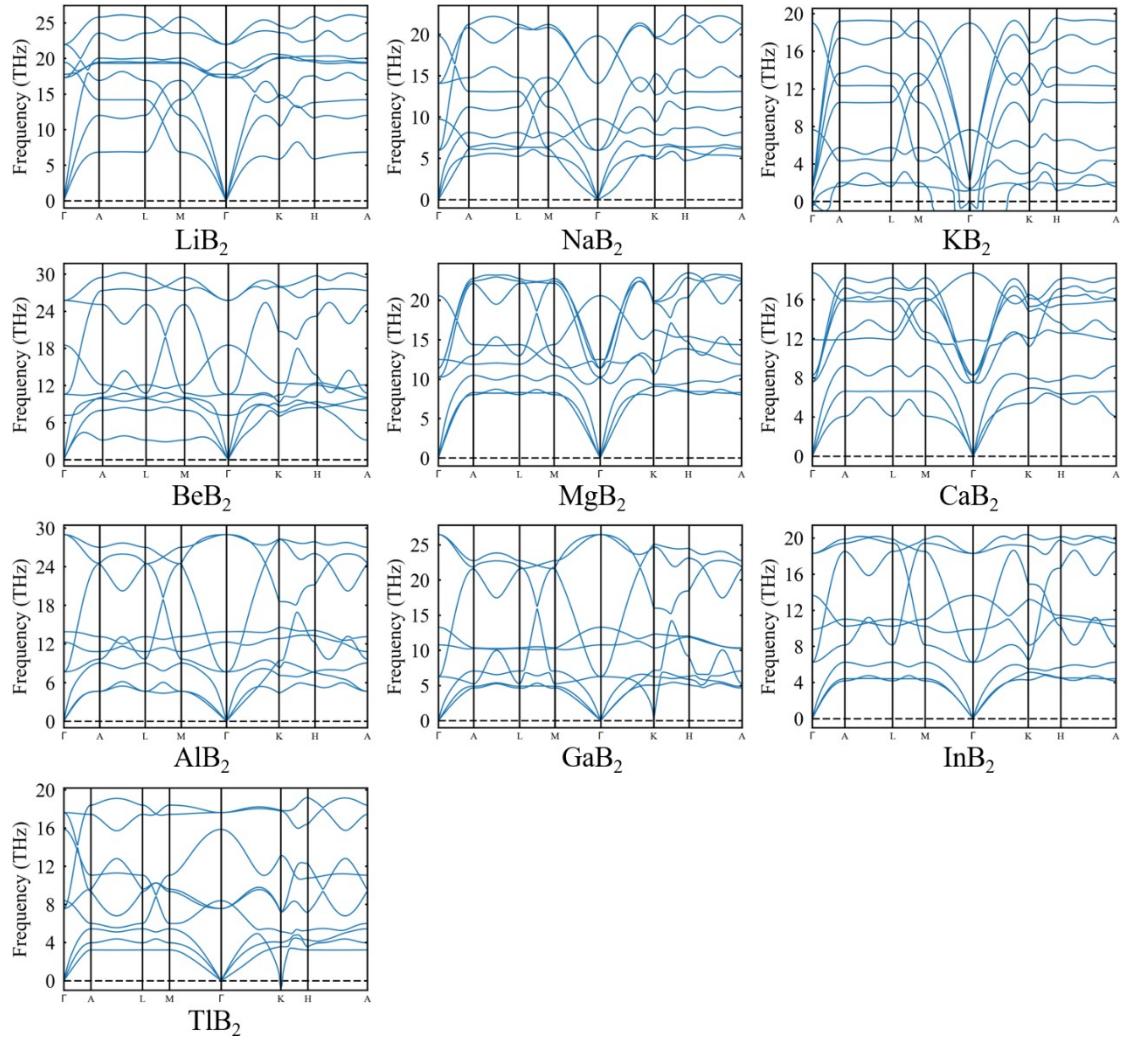
**Fig. S1.** Phonon spectra along the high symmetry directions for bulk MB$_2$.
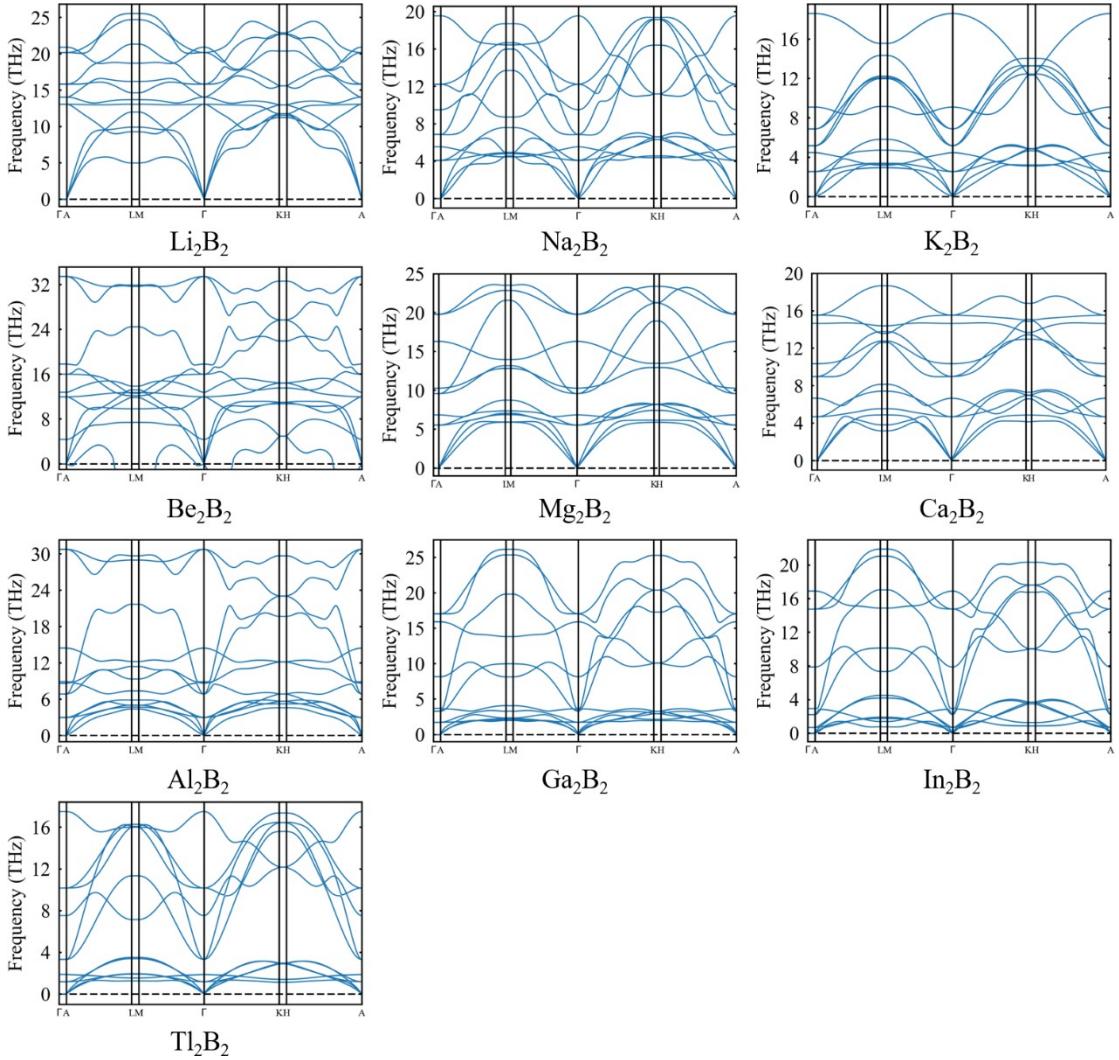
Fig. S2. Phonon spectra along the high symmetry directions for M_2B_2 monolayers.

2. Mechanical stabilities and properties of M_2B_2 monolayers

For a 2D hexagonal crystal, there are two independent elastic constants, namely c_{11} and c_{12}. The stiffness tensor c_{ij} can be obtained using the following equation,

$$E = \frac{1}{2}c_{11}\varepsilon_{xx}^2 + \frac{1}{2}c_{22}\varepsilon_{yy}^2 + c_{12}\varepsilon_{xx}\varepsilon_{yy} \tag{1}$$

Where E is the elastic strain energy, ε_{xx} and ε_{yy} are the tensile strains along x-direction

and y-direction, respectively. Applying uniaxial stain ε_0 along x-direction leads to $\varepsilon_{yy} = 0$ and $E = \frac{1}{2}c_{11}\varepsilon_{xx}^2$ and then the c_{11} is two times of the coefficient of the quadratic term obtained by fitting $E(\varepsilon_0)$ as a function of ε_0 with a quadratic polynomial. Similarly, applying equibiaxial strain ε_0 leads to $\varepsilon_{xx} = \varepsilon_{yy}$ and then the c_{11} can be acquired by fitting $E = (\frac{1}{2}c_{11} + \frac{1}{2}c_{22} + c_{12})\varepsilon_{xx}^2$. In the end, $c_{66} = \frac{1}{2}(c_{11} - c_{12})$. The mechanically stable 2D hexagonal crystal must satisfy $c_{11} > 0$ and $c_{11} > |c_{12}|$. Young's modulus is defined by

$$E = \frac{c_{11}^2 - c_{12}^2}{c_{11}}$$

representing the strain response in the direction of applied uniaxial stress. The shear modulus is defined by $G = c_{66}$ for 2D hexagonal crystals reflecting the rigidity of lattice to shear stress. The Poisson's ratio is defined by $\mu = \frac{c_{12}}{c_{11}}$ representing the ratio of transverse contraction to longitudinal expansion of lattice in the stretching force direction. In this work, we applied the strain ε from -1.5% to 1.5% by the interment of 0.5% to calculate the elastic constants. The results of mechanical properties of MBenes (M = Li, Na, K, Be, Mg, Ca, Al, Ga, In, Tl) are plotted in Fig. S3 and Fig. S4 and listed in Table S1.
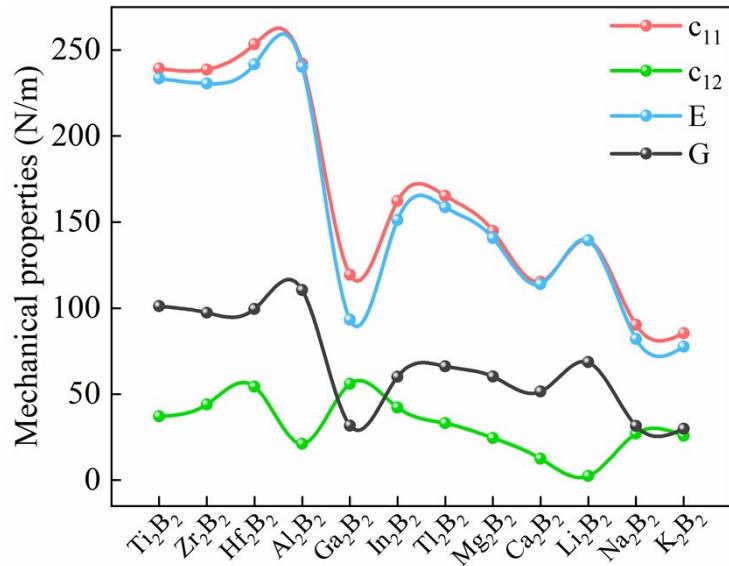
Fig. S3. Mechanical properties (N/m) of hexagonal M_2B_2 monolayers including elastic constants (c_{ij}), Young's modulus (E) and shear modulus (G).
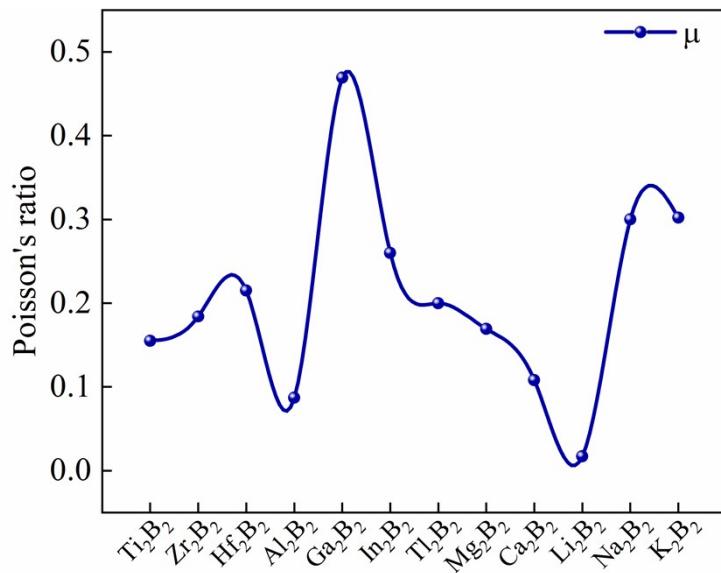

Fig. S4. The Poisson's ratio (μ) of hexagonal M_2B_2 monolayers.

Table S1. Elastic constants (c_{ij}, N/m), Young's modulus (E, N/m), shear modulus (G, N/m) and Poisson's ratio (μ) of M_2B_2 monolayers.

formula	c_{11}	c_{12}	c_{66}	Young's modulus E	Shear modulus G	Poisson's ratio μ
Al_2B_2	242	21	110	240	110	0.09
Ga_2B_2	119	56	32	93	32	0.47
In_2B_2	162	42	60	151	60	0.26
Tl_2B_2	165	33	66	159	66	0.20
Mg_2B_2	145	24	60	141	60	0.17
Ca_2B_2	115	12	51	114	51	0.11
Li_2B_2	139	2	69	139	69	0.02
Na_2B_2	90	27	32	82	32	0.30
K_2B_2	85	26	30	78	30	0.30
Ti_2B_2	239	37	101	234	101	0.16
Zr_2B_2	239	44	97	230	97	0.18
Hf_2B_2	253	54	99	242	99	0.22

3. Exfoliation of MB$_2$ and M$_2$B$_2$ monolayers

The exfoliation energies of MB$_2$ and M$_2$B$_2$ monolayers are calculated according

to the following equation,

$$E_{exf} = (E_{exfMB_2} - E_{MB_2})/2S$$

(2)

where E_{MB_2} and E_{exfMB_2} represent the total energies of bulk MB$_2$ and exfoliated MB$_2$,

respectively. S represents the area of exfoliation surfaces of MB$_2$.
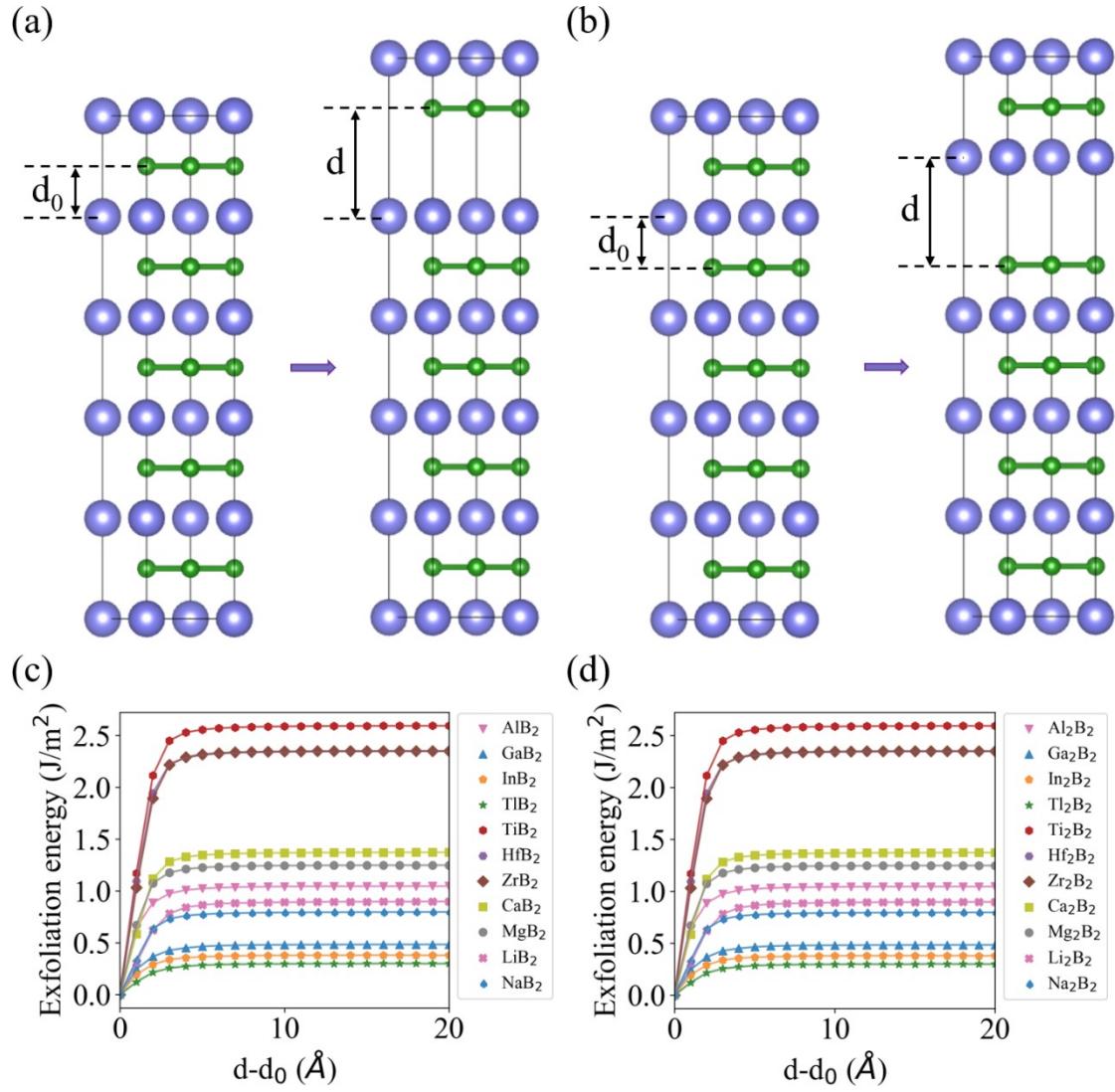
Fig. S5. Schematic diagrams of exfoliation for (a) MB_2 and (b) M_2B_2 monolayers and exfoliation energies of (c) MB_2 and (d) M_2B_2 monolayers. d_0 and d represent the distance between metal and boron layers in the original bulk MB_2 and the distance between the monolayer and the remaining piece of MB_2 after exfoliation, respectively.

Table S2. Exfoliation energies (J/m^2) of MB_2 and M_2B_2 monolayers.

M element	M_2B_2	MB_2
Ti	2.59374	2.59375
Zr	2.35128	2.35125

|		
Hf	2.34809	2.34796
Ca	1.37238	1.37236
Mg	1.24836	1.24839
Al	1.04623	1.04622
Li	0.89686	0.89687
Na	0.79645	0.79645
Ga	0.48395	0.48391
In	0.38101	0.38079
Tl	0.29986	0.29984
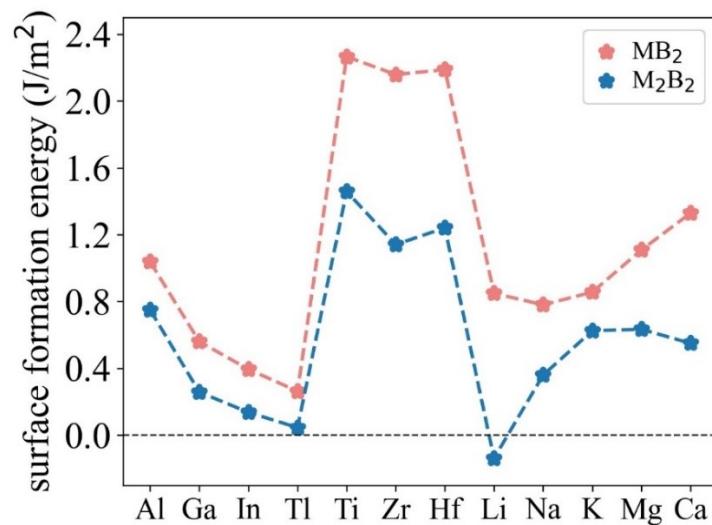
Fig. S6. Surface formation energies (J/m^2) of MB$_2$ and M$_2$B$_2$ monolayers.

Table S3. Surface formation energies (J/m^2) of M$_2$B$_2$ and MB$_2$ monolayers and corresponding bulk M energies (eV/atom) used in the calculations of surface formation energies.

M	surface formation energy of M$_2$B$_2$	surface formation energy of MB$_2$	bulk M energy
Al	0.750	1.038	-4.085
Ga	0.258	0.561	-3.196
In	0.137	0.395	-2.883
Tl	0.046	0.264	-2.547
Ti	1.458	2.266	-8.435

Zr	1.141	2.158	-9.056
Hf	1.241	2.188	-10.381
Li	-0.138	0.849	-2.083
Na	0.360	0.781	-1.472
K	0.625	0.856	-1.162
Mg	0.634	1.109	-1.795
Ca	0.550	1.329	-2.166

4. Thermal stabilities of Mg_2B_2 and Ca_2B_2 monolayers
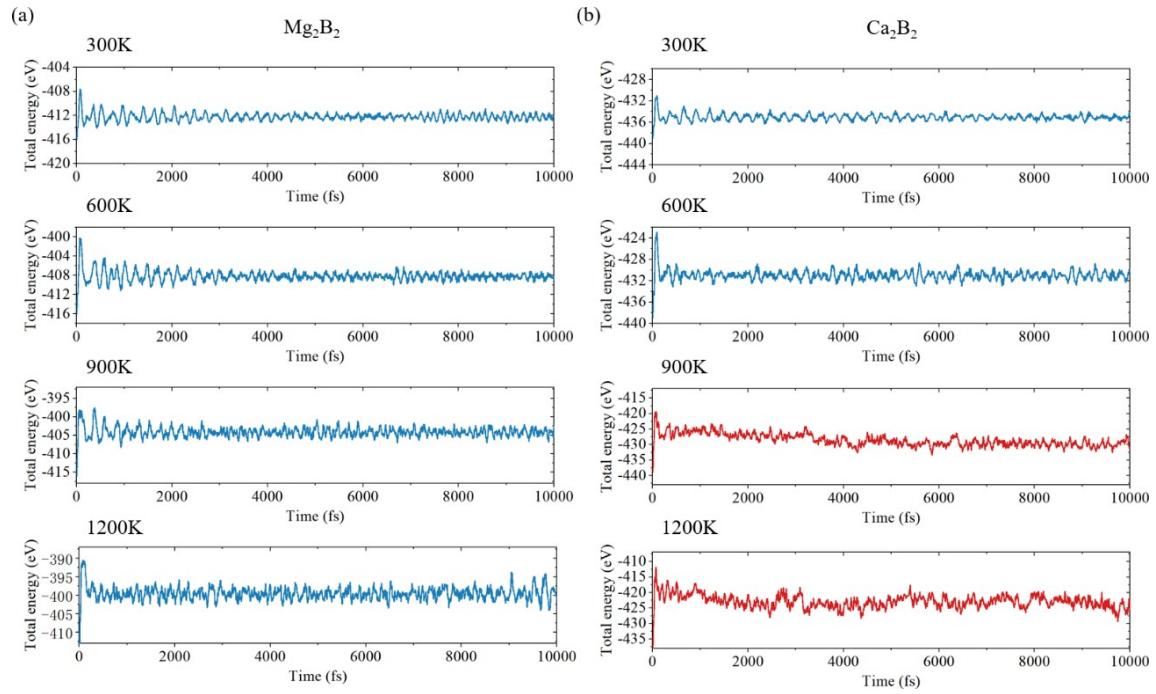

Fig. S7. Total energy fluctuations of (a) Mg_2B_2 and (b) Ca_2B_2 in the AIMD simulation at 300 K, 600K, 900 K and 1200 K for 10 ps.
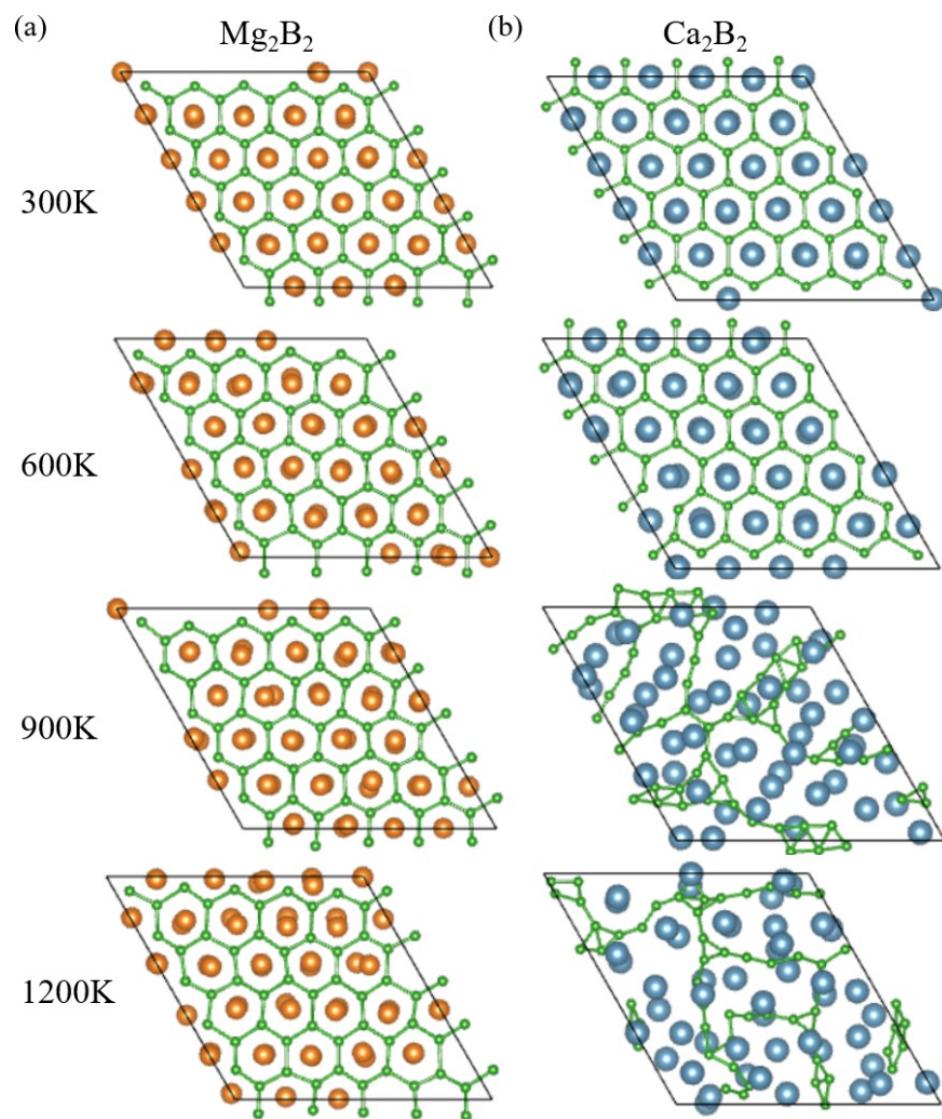
Fig. S8. Snapshots of (a) Mg_2B_2 and (b) Ca_2B_2 in the AIMD simulation at 300 K, 600K, 900 K and 1200 K for 10 ps.

5. HSE06 functional calculations
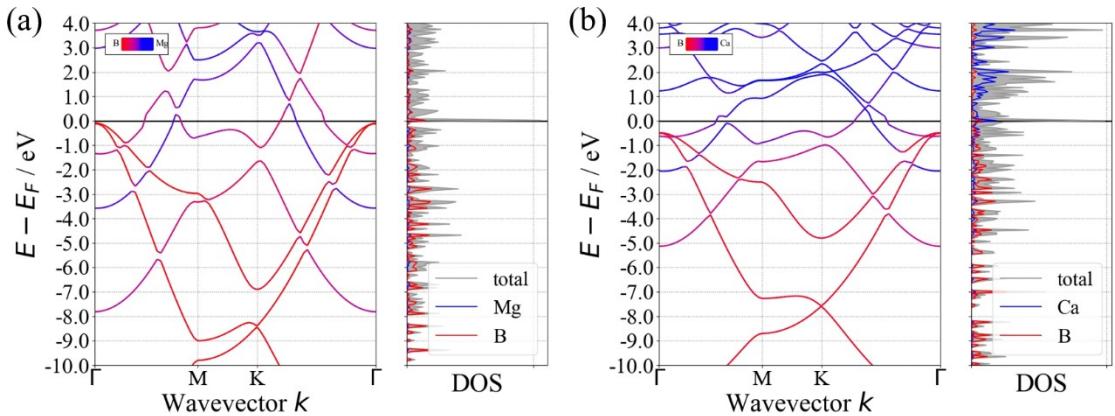
Fig. S9. HSE06 projected electronic band structures and DOS of (a) Mg_2B_2 and (b) Ca_2B_2 monolayers.

## 6. Li/Na adsorption on Mg_2B_2 and Ca_2B_2 monolayers
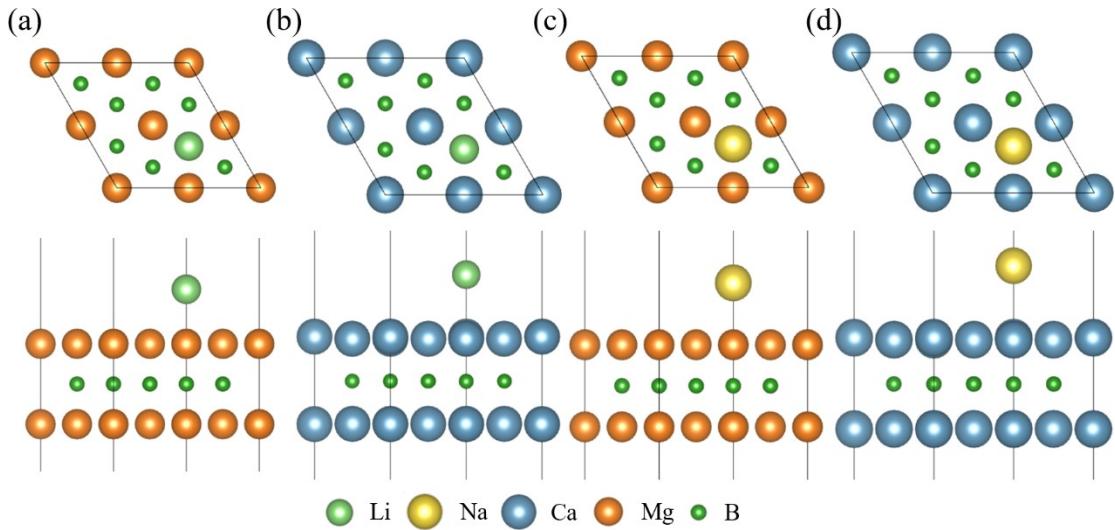
Fig. S10. Configurations of $Li_{0.25}/Na_{0.25}M_2B_2$ for the most stable sites. The hollow site is the favorable site for Li/Na ions on the surfaces of Mg_2B_2 and Ca_2B_2.
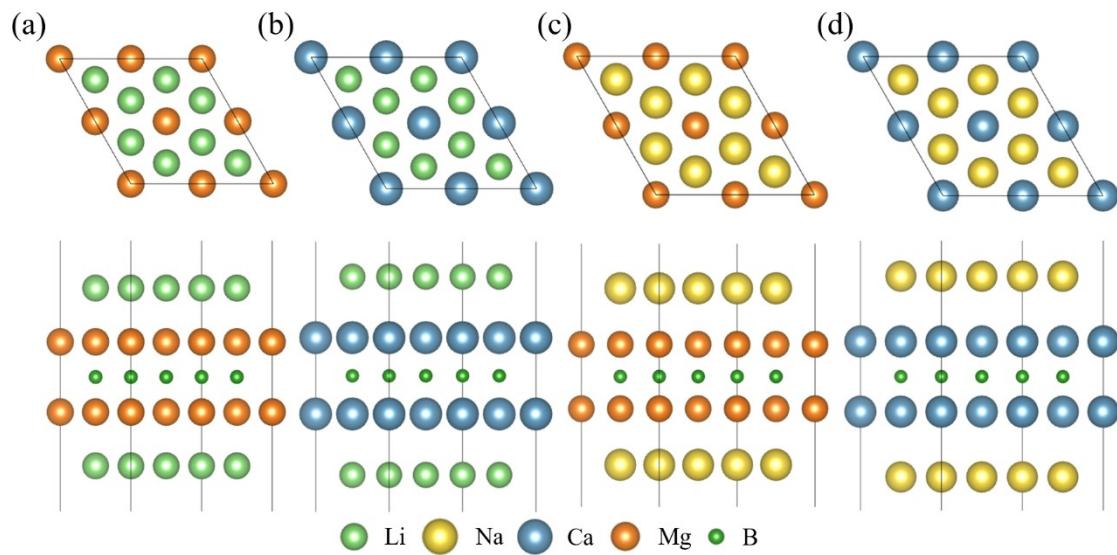
Fig. S11. Configurations of $Li_4/Na_4M_2B_2$ for the hollow sites. All these configures possess positive adsorption energies.

Table S4. Average adsorption energies (E_{ave}) of the $Li_4/Na_4M_2B_2$ and $Li_2/Na_2M_2B_2$ configurations.

configuration	E_{ave} (x=4)	E_{ave} (x=2)
$Li_xCa_2B_2$	0.794	-0.279
$Li_xMg_2B_2$	0.928	-0.431
$Na_xCa_2B_2$	1.931	-0.345
$Na_xMg_2B_2$	2.554	-0.272
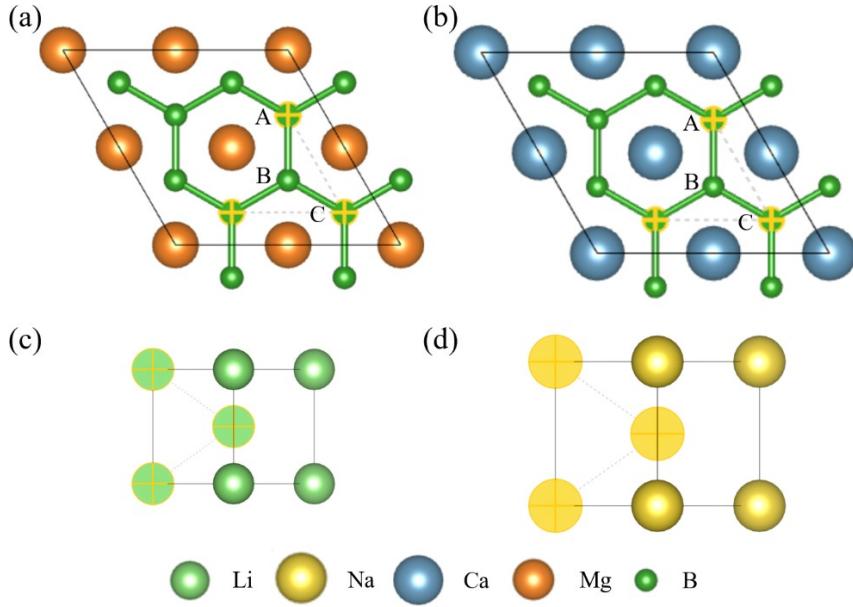
Fig. S12. Comparison of the (0 0 1) crystallographic planes of (a) Mg_2B_2 and (b) Ca_2B_2 and the (1 1 0) crystal planes of body-centered cubic (c) Li and (d) Na. The concerned S1 sites and S1-S1-S1 angles are labeled by yellow crosses.

Table S5. Mismatching ratios between d_{A-C} and d_{b-c}.

	Li_{bcc} (1 1 0)	Na_{bcc} (1 1 0)
MgB (0 0 1)	2.7%	-16.4%
CaB (0 0 1)	11.2%	-8.4%

Table S6. Mismatching ratios between d_{A-B} and d_{b-c}.

	Li_{bcc} (1 1 0)	Na_{bcc} (1 1 0)
MgB (0 0 1)	-40.7%	-51.2%
CaB (0 0 1)	-35.8%	-47.1%
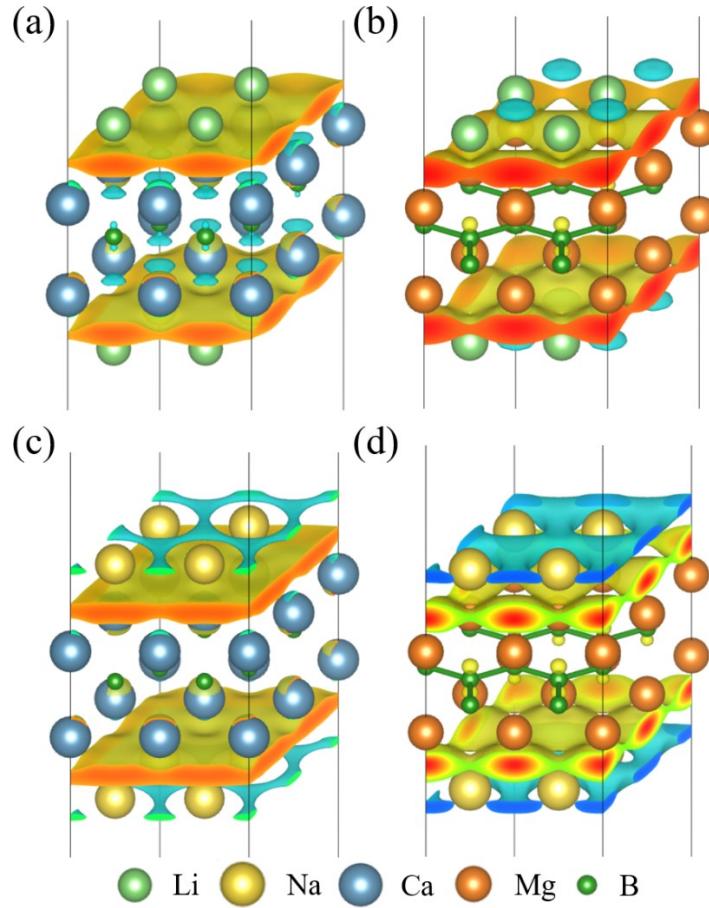
Fig. S13. Charge difference densities of the (a) $Li_2Ca_2B_2$, (b) $Li_2Mg_2B_2$, (c) $Na_2Ca_2B_2$ and (d) $Na_2Mg_2B_2$ configurations. The yellow and blue cloud areas represent electron gains and losses.

Table S7. Distances between the ion layers and the monolayers (d_1, in Å), thicknesses of the monolayers (d_2, in Å), bond lengths of M-M (l_{M-M}, in Å), M-B (l_{M-B}, in Å) and B-B (l_{B-B}, in Å), cross-section areas (S_{cross}, in Å^2), S_{cross} change ratios and average adsorption energies (E_{ave}, in eV) of different configurations.

configuration	d_1	d_2	l_{M-M}	l_{M-B}	l_{B-B}	S_{cross}	S_{cross} change ratio	E_{ave}
Ca_2B_2		3.714	3.333	2.674	1.924	38.485		

Mg_2B_2		3.393	3.078	2.457	1.777	32.825		
$LiCa_2B_2$	2.828	3.740	3.318	2.681	1.915	38.128	-0.9%	-0.266
$Li_2Ca_2B_2$	2.769	3.780	3.307	2.687	1.909	37.891	-1.5%	-0.275
$NaCa_2B_2$	3.235	3.715	3.354	2.685	1.937	38.974	1.3%	-0.333
$Na_2Ca_2B_2$	3.231	3.725	3.367	2.692	1.944	39.282	2.1%	-0.345
$LiMg_2B_2$	2.367	3.363	3.084	2.459	1.781	32.954	0.4%	-0.399
$Li_2Mg_2B_2$	2.362	3.367	3.086	2.451	1.781	32.980	0.5%	-0.431
$NaMg_2B_2$	2.860	3.293	3.133	2.442	1.809	33.996	3.6%	-0.250
$Na_2Mg_2B_2$	2.855	3.309	3.153	2.460	1.820	34.441	4.9%	-0.272
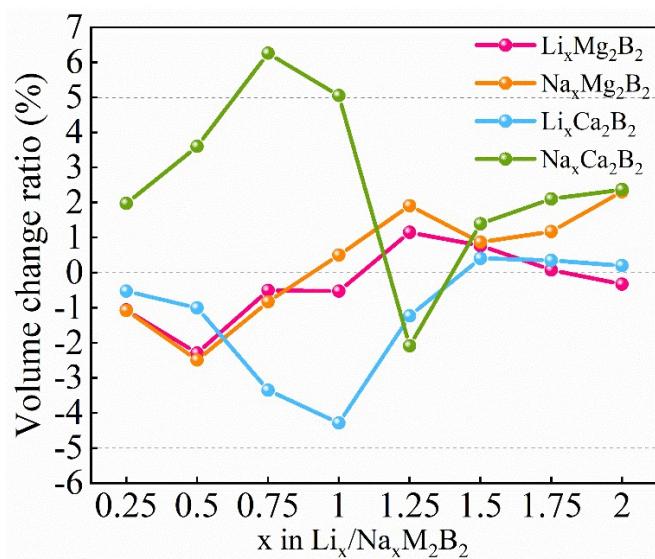
Fig. S14. Volume change ratios (γ) of the $Li_x/Na_xM_2B_2$ configurations at different Li/Na concentrations (x, from 0 to 2 by step 0.25).

7. Electronic structures of Mg$_2$B$_2$ and Ca$_2$B$_2$ monolayers adsorbed with Li/Na ions
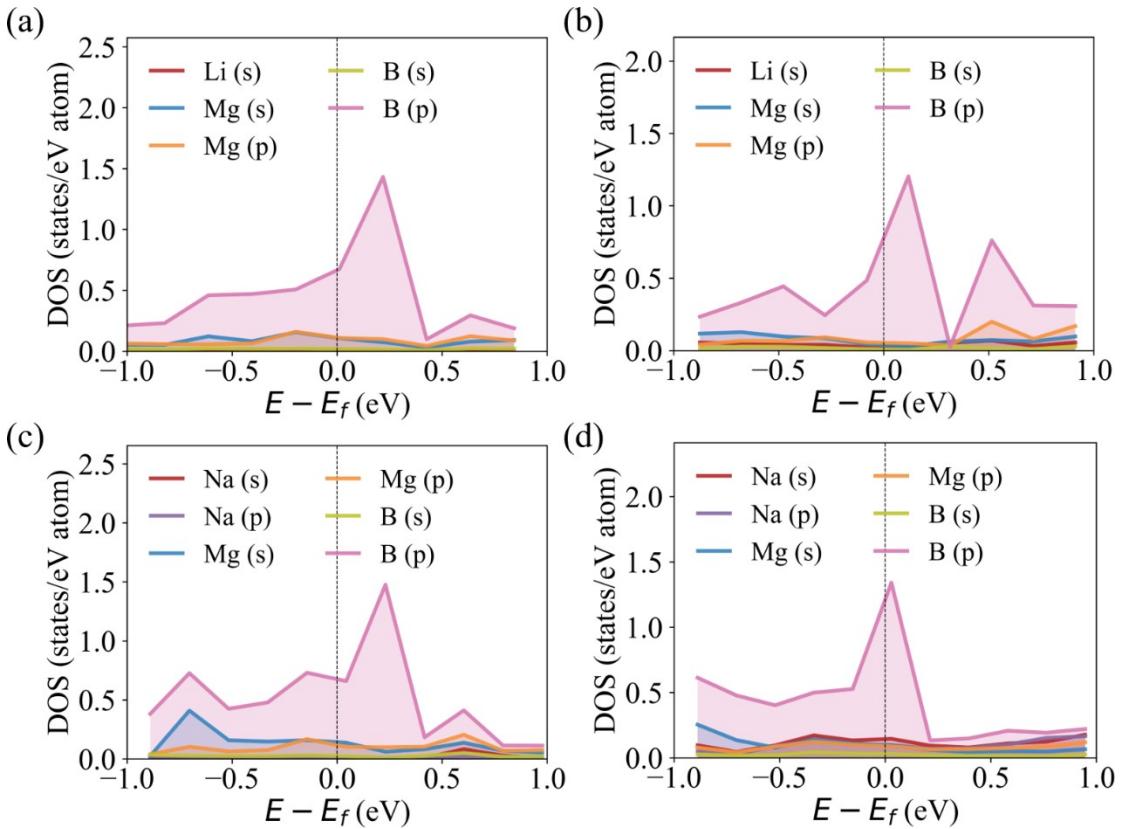
Fig. S15. Elemental projected DOS of the Mg$_2$B$_2$ monolayer adsorbed with (a) one single Li atom, (b) one layer of Li atoms, (c) one single Na atom, and (d) one layer of Na atoms, respectively. The Fermi energy levels are set as zero.
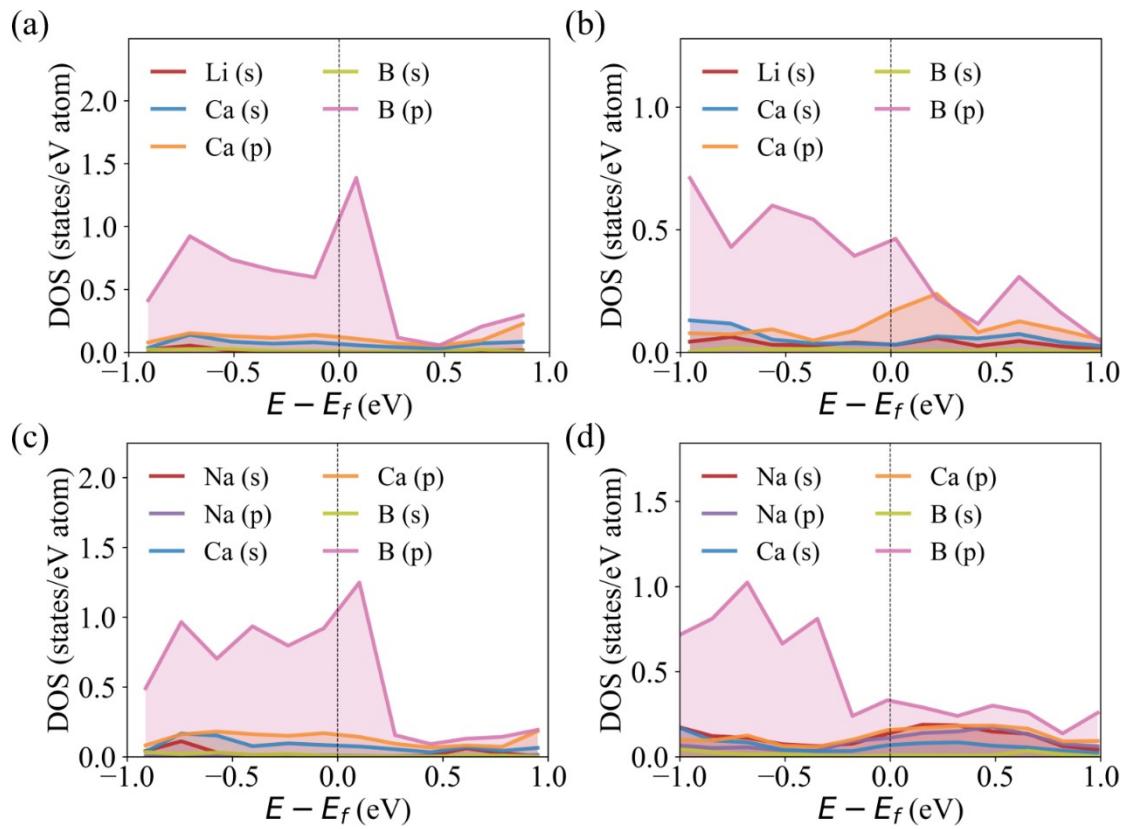
Fig. S16. Elemental projected DOS of the Ca_2B_2 monolayer adsorbed with (a) one single Li atom, (b) one layer of Li atoms, (c) one single Na atom, and (d) one layer of Na atoms, respectively. The Fermi energy levels are set as zero.

8. Li/Na diffusion on Mg_2B_2 and Ca_2B_2 monolayers

Table S8. Diffusion energy barriers ($E_{barrier}$) and diffusivities (D) of Li/Na on IIA metal MBene monolayers, transition metal MBene monolayers and Graphene.

	Li		Na	
	$E_{barrier}$ (meV)	D (cm^2/s)	$E_{barrier}$ (meV)	D (cm^2/s)
Ca_2B_2	16	3.7E-03	12	4.3E-03
Mg_2B_2	27	2.6E-03	14	4.3E-03
Sc_2B_2[1]	3	3.0E-04	--	--

17

Ti$_2$B$_2$[2]	4	2.6E-04	--	--
Zr$_2$B$_2$[3]	4	2.8E-04	--	--
Y$_2$B$_2$[4]	13	1.0E-02	8	1.3E-02
Graphene[5]	300	6.0E-07	--	--

9. Comparison with other anode materials

Table S9. Diffusion energy barriers (E$_{barrier}$), specific capacities (C) and average open circuit voltages (V$_{ave}$) of Li on IIA metal MBene monolayers, transition metal MBene monolayers, Ti$_3$C$_2$, and Graphite.

monolayer	E$_{barrier}$ (meV)	C (mAh/g)	V$_{ave}$ (V)
Mg$_2$B$_2$	27	764	0.395
Ca$_2$B$_2$	16	527	0.275
Zr$_2$B$_2$[3]	17	526	0.236
Sc$_2$B$_2$[1]	3	480	0.410
Ti$_2$B$_2$[2]	17	456	0.526
Fe$_2$B$_2$[6]	240	665	0.330
Mo$_2$B$_2$[6]	270	444	0.410
Ti$_3$C$_2$[7]	70	448	0.413
Graphite[8]	450-1200	372	--

Table S10. Diffusion energy barriers (E$_{barrier}$), specific capacities (C) and average open circuit voltages (V$_{ave}$) of Na on IIA metal MBene monolayers, transition metal MBene monolayers, Ti$_3$C$_2$, MoS$_2$, BCN, and Graphene.

monolayer	E$_{barrier}$ (meV)	C (mAh/g)	V$_{ave}$ (V)
Mg$_2$B$_2$	14	859	0.279
Ca$_2$B$_2$	12	527	0.362
MoC$_2$[9]	230	447	0.280
Ti$_2$B$_2$[2]	8	342	0.502
Ti$_3$C$_2$[7]	96	352	0.137
MoS$_2$[10]	280	146	0.750

BCN[11]	260	647	0.340
Graphene[5]	130	--	--

10. Anode performance of multilayers
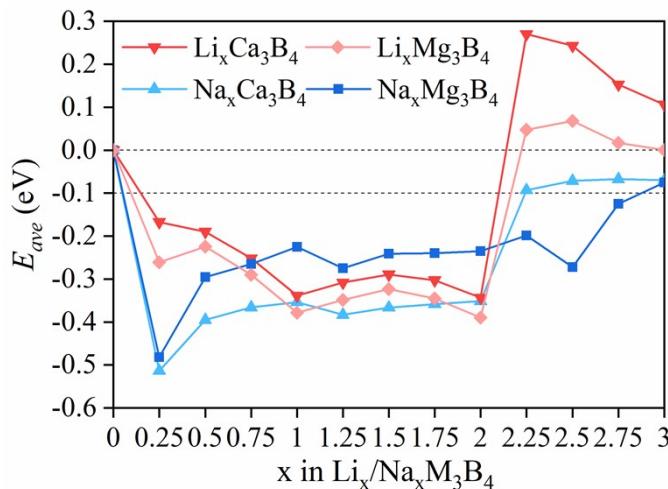
Fig. S17. Average adsorption energies (E_{ave}) of the $Li_x/Na_xM_3B_4$ configurations at different Li/Na concentrations (x, from 0 to 3 by step 0.25). The configurations with values of E_{ave} in the range of -0.1 to 0 eV are considered to be energetically unstable.
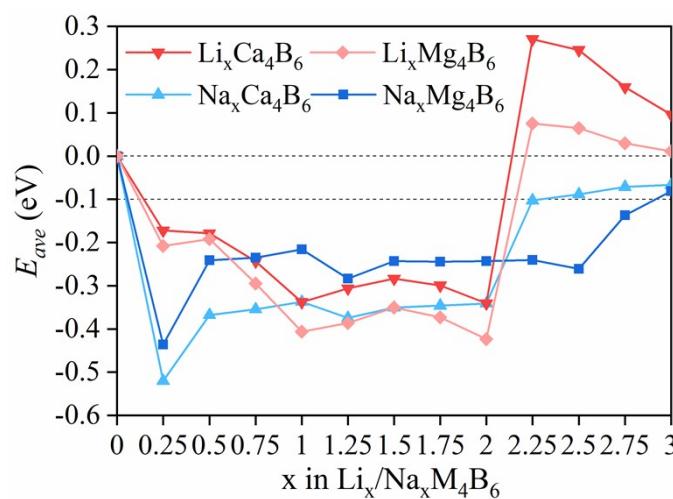
**Fig. S18.** Average adsorption energies (E_{ave}) of the $Li_x/Na_xM_4B_6$ configurations at different Li/Na concentrations (x, from 0 to 3 by step 0.25). The configurations with

values of E_{ave} in the range of -0.1 to 0 eV are considered to be energetically unstable.

Table S11. The energy differences (eV) of E_{ave} between the $Li_x/Na_xM_3B_4$ and $Li_x/Na_xM_2B_2$ configurations.

x	$Li_xCa_3B_4$	$NaxCa_3B_4$	$Li_xMg_3B_4$	$Na_xMg_3B_4$
0	0.000	0.000	0.000	0.000
0.25	-0.065	-0.037	0.026	0.050
0.5	-0.047	0.031	-0.016	-0.014
0.75	-0.056	-0.017	0.004	-0.017
1	-0.073	-0.021	0.021	0.025
1.25	-0.073	-0.022	0.010	0.023
1.5	-0.061	-0.011	0.026	0.016
1.75	-0.056	-0.010	0.031	0.020
2	-0.068	-0.006	0.041	0.037
2.25	0.024	-0.090	-0.104	-0.085
2.5	0.144	-0.004	0.049	-0.193
2.75	0.190	0.024	0.080	-0.068
3	0.262	0.063	0.165	-0.015

Table S12. The energy differences (eV) of E_{ave} between the $Li_x/Na_xM_4B_6$ and $Li_x/Na_xM_2B_2$ configurations.

x	$Li_xCa_4B_6$	$NaxCa_4B_6$	$Li_xMg_4B_6$	$Na_xMg_4B_6$
0	0.000	0.000	0.000	0.000
0.25	-0.070	-0.044	0.079	0.096
0.5	-0.036	0.058	0.017	0.040
0.75	-0.048	-0.005	-0.001	0.013
1	-0.072	-0.004	-0.008	0.034
1.25	-0.071	-0.013	-0.028	0.015
1.5	-0.055	0.005	-0.001	0.014
1.75	-0.053	0.002	0.003	0.016
2	-0.066	0.004	0.007	0.029
2.25	0.025	-0.099	-0.076	-0.127
2.5	0.147	-0.022	0.046	-0.181
2.75	0.197	0.020	0.092	-0.080

3	0.252	0.067	0.175	-0.021
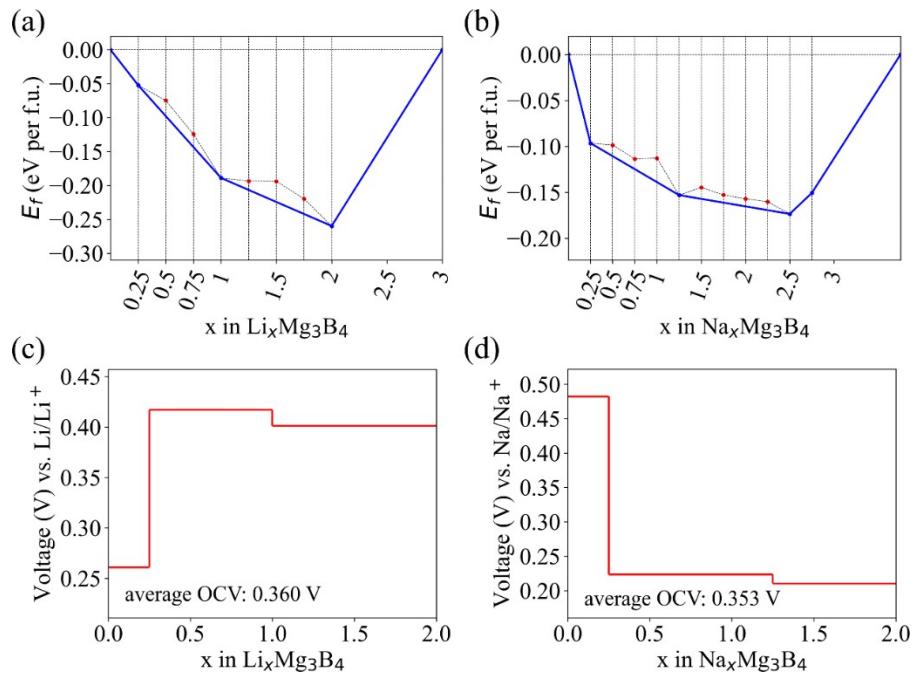
Fig. S19. The convex hulls of E_f for (a) $Li_xMg_3B_4$ and (b) $Na_xMg_3B_4$ configurations

and OCV profiles of (c) $Li_xMg_3B_4$ against Li/Li+ and (d) $Na_xMg_3B_4$ against Na/Na+.
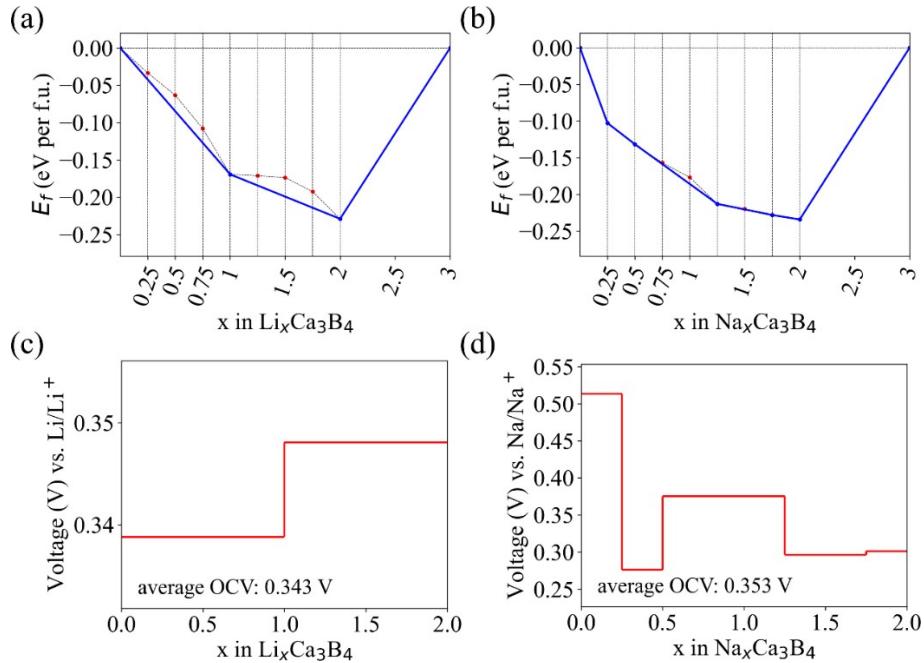
Fig. S20. The convex hulls of E_f for (a) $Li_xCa_3B_4$ and (b) $Na_xCa_3B_4$ configurations and OCV profiles of (c) $Li_xCa_3B_4$ against Li/Li+ and (d) $Na_xCa_3B_4$ against Na/Na+.
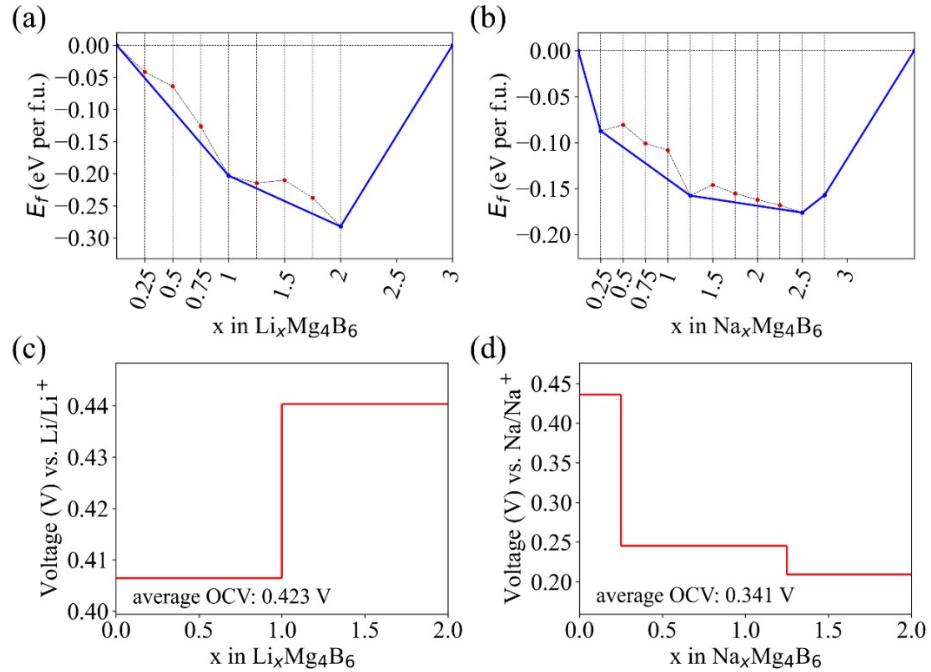
Fig. S21. The convex hulls of E_f for (a) $Li_xMg_4B_6$ and (b) $Na_xMg_4B_6$ configurations and OCV profiles of (c) $Li_xMg_4B_6$ against Li/Li+ and (d) $Na_xMg_4B_6$ against Na/Na+.
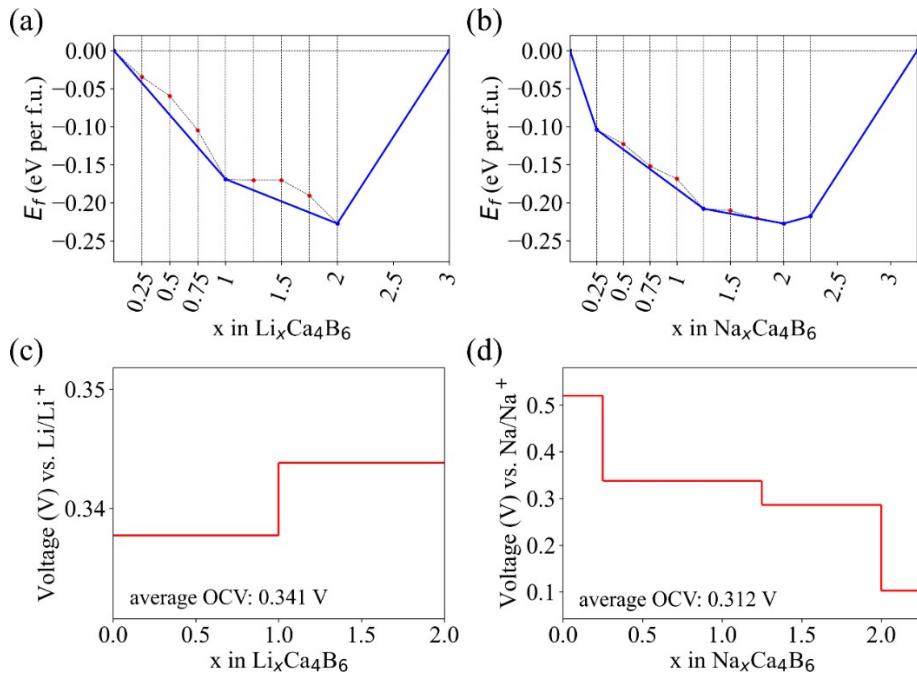
Fig. S22. The convex hulls of E_f for (a) $Li_xCa_4B_6$ and (b) $Na_xCa_4B_6$ configurations and OCV profiles of (c) $Li_xCa_4B_6$ against Li/Li+ and (d) $Na_xCa_4B_6$ against Na/Na+.
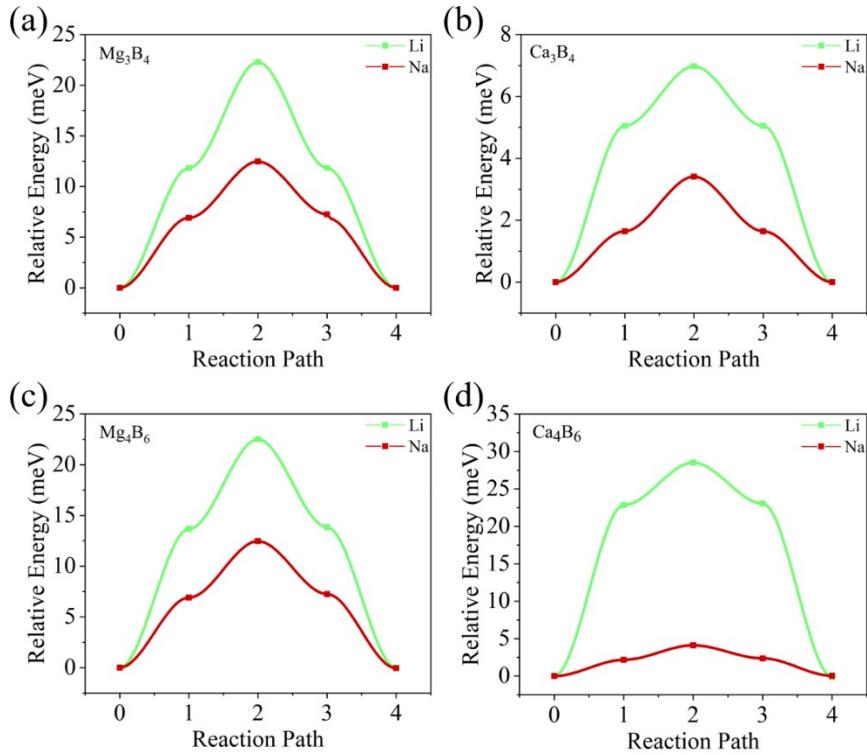
Fig. S23. The Li/Na diffusion energy barriers (meV) for (a) Mg_3B_4, (b) Ca_3B_4 (c) Mg_4B_6 and (d) Ca_4B_6 multilayers.

11. Effect of functionalization
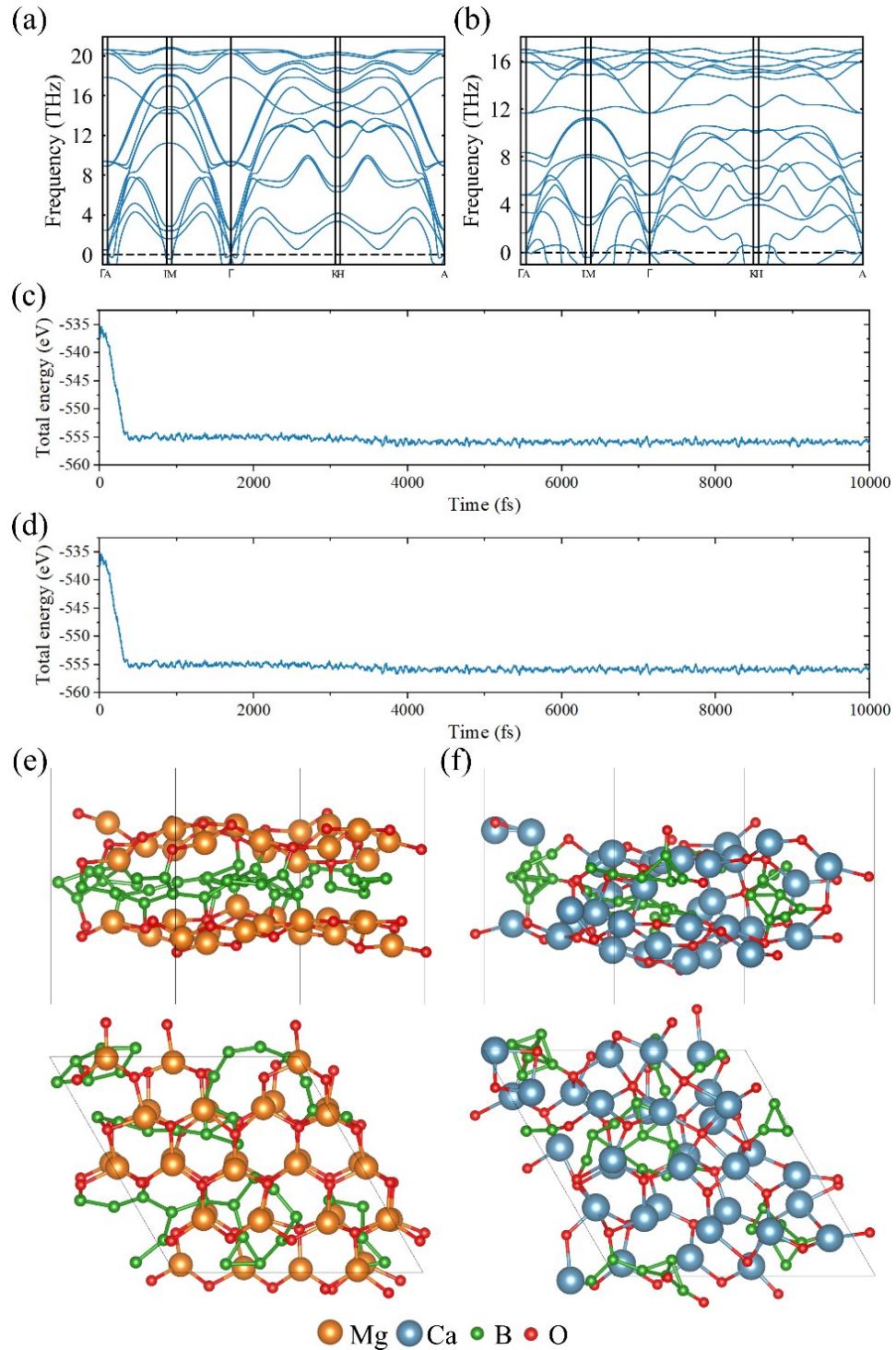
Fig. S24. Phonon spectra along the high symmetry directions for (a) Mg$_2$B$_2$O$_2$ and (b)

Ca$_2$B$_2$O$_2$. Total energy fluctuations of (c) Mg$_2$B$_2$O$_2$ and (d) Ca$_2$B$_2$O$_2$ in the AIMD

simulation at 300 K for 10 ps and the corresponding structure snapshots of (e) Mg$_2$B$_2$O$_2$

and (f) Ca$_2$B$_2$O$_2$.

Appendix

The POSCARs and CONTCARs for fully lithiated and sodiated Mg$_2$B$_2$ and Ca$_2$B$_2$:

Li8 Mg8 B8 (POSCAR)
1.00000000000000
   6.1710360018532819   0.0000000062764495   0.0000000000000000

  -3.0855120015850690   5.3442746302461277   0.0000000000000000
   0.0000000000000000   0.0000000000000000   33.0505128388136953

  Li   Mg   B
   8   8   8
Direct
  0.3333340000000007   0.1666659999999993   0.6223978493336166
  0.3333340000000007   0.6666659999999993   0.6223978493336166
  0.8333340000000007   0.1666659999999993   0.6223978493336166
  0.8333340000000007   0.6666659999999993   0.6223978493336166
  0.3333340000000007   0.1666659999999993   0.3776021506663834
  0.3333340000000007   0.6666659999999993   0.3776021506663834
  0.8333340000000007   0.1666659999999993   0.3776021506663834
  0.8333340000000007   0.6666659999999993   0.3776021506663834
  0.0000000000000000   0.0000000000000000   0.4490690701310235
  0.0000000000000000   0.5000000000000000   0.4490690701310235
  0.5000000000000000   0.0000000000000000   0.4490690701310235

0.5000000000000000	0.5000000000000000	0.4490690701310235
0.0000000000000000	0.0000000000000000	0.5509309298689765
0.0000000000000000	0.5000000000000000	0.5509309298689765
0.5000000000000000	0.0000000000000000	0.5509309298689765
0.5000000000000000	0.5000000000000000	0.5509309298689765
0.3333340000000007	0.1666659999999993	0.5000000000000000
0.3333340000000007	0.6666659999999993	0.5000000000000000
0.8333340000000007	0.1666659999999993	0.5000000000000000
0.8333340000000007	0.6666659999999993	0.5000000000000000
0.1666659999999993	0.3333340000000007	0.5000000000000000
0.1666659999999993	0.8333340000000007	0.5000000000000000
0.6666659999999993	0.3333340000000007	0.5000000000000000
0.6666659999999993	0.8333340000000007	0.5000000000000000

Li8 Mg8 B8 (CONTCAR)

   1.00000000000000

6.1710337692259110	0.0000000062739385	0.0000000000000000
-3.0855108852757263	5.3442726967346150	0.0000000000000000
0.0000000000000000	0.0000000000000000	33.0505128388136953

   Li   Mg   B
    8   8   8

Direct

0.3333340000000007	0.1666659999999993	0.6223961020882811
0.3333340000000007	0.6666659999999993	0.6223961020882811
0.8333340000000007	0.1666659999999993	0.6223961020882811
0.8333340000000007	0.6666659999999993	0.6223961020882811
0.3333340000000007	0.1666659999999993	0.3776038979117189
0.3333340000000007	0.6666659999999993	0.3776038979117189

0.8333340000000007	0.1666659999999993	0.3776038979117189
0.8333340000000007	0.6666659999999993	0.3776038979117189
0.0000000000000000	0.0000000000000000	0.4490700066170774
0.0000000000000000	0.5000000000000000	0.4490700066170774
0.5000000000000000	0.0000000000000000	0.4490700066170774
0.5000000000000000	0.5000000000000000	0.4490700066170774
0.0000000000000000	0.0000000000000000	0.5509299933829226
0.0000000000000000	0.5000000000000000	0.5509299933829226
0.5000000000000000	0.0000000000000000	0.5509299933829226
0.5000000000000000	0.5000000000000000	0.5509299933829226
0.3333340000000007	0.1666659999999993	0.5000000000000000
0.3333340000000007	0.6666659999999993	0.5000000000000000
0.8333340000000007	0.1666659999999993	0.5000000000000000
0.8333340000000007	0.6666659999999993	0.5000000000000000
0.1666659999999993	0.3333340000000007	0.5000000000000000
0.1666659999999993	0.8333340000000007	0.5000000000000000
0.6666659999999993	0.3333340000000007	0.5000000000000000
0.6666659999999993	0.8333340000000007	0.5000000000000000

Li8 Ca8 B8 (POSCAR)

1.00000000000000

6.6155715783610543	-0.0000001262391976	0.0000000000000000
-3.3077725841691019	5.7292580307680225	0.0000000000000000
0.0000000000000000	0.0000000000000000	33.3047817894384721

Li	Ca	B
8	8	8

Direct

0.3333340000000007	0.1666659999999993	0.3601218216550399
0.3333340000000007	0.6666659999999993	0.3601218216550399

```
0.8333340000000007    0.1666659999999993    0.3601218216550399
0.8333340000000007    0.6666659999999993    0.3601218216550399
0.3333340000000007    0.1666659999999993    0.6398781783451165
0.3333340000000007    0.6666659999999993    0.6398781783451165
0.8333340000000007    0.1666659999999993    0.6398781783451165
0.8333340000000007    0.6666659999999993    0.6398781783451165
0.0000000000000000    0.0000000000000000    0.4432636271042920
0.0000000000000000    0.5000000000000000    0.4432636271042920
0.5000000000000000    0.0000000000000000    0.4432636271042920
0.5000000000000000    0.5000000000000000    0.4432636271042920
0.0000000000000000    0.0000000000000000    0.5567363728956298
0.0000000000000000    0.5000000000000000    0.5567363728956298
0.5000000000000000    0.0000000000000000    0.5567363728956298
0.5000000000000000    0.5000000000000000    0.5567363728956298
0.3333340000000007    0.1666659999999993    0.5000000000000000
0.3333340000000007    0.6666659999999993    0.5000000000000000
0.8333340000000007    0.1666659999999993    0.5000000000000000
0.8333340000000007    0.6666659999999993    0.5000000000000000
0.1666659999999993    0.3333340000000007    0.5000000000000000
0.1666659999999993    0.8333340000000007    0.5000000000000000
0.6666659999999993    0.3333340000000007    0.5000000000000000
0.6666659999999993    0.8333340000000007    0.5000000000000000
```

Li8 Ca8 B8 (CONTCAR)
   1.00000000000000
     6.6145515361117964   -0.0000001285509600   0.0000000000000000
    -3.3072625670994329   5.7283746471474082   0.0000000000000000
     0.0000000000000000   0.0000000000000000   33.3047817894384721

   Li   Ca   B

```
        8       8       8
Direct
  0.3333340000000007    0.1666659999999993    0.3601212273169622
  0.3333340000000007    0.6666659999999993    0.3601212273169622
  0.8333340000000007    0.1666659999999993    0.3601212273169622
  0.8333340000000007    0.6666659999999993    0.3601212273169622
  0.3333340000000007    0.1666659999999993    0.6398787726831945
  0.3333340000000007    0.6666659999999993    0.6398787726831945
  0.8333340000000007    0.1666659999999993    0.6398787726831945
  0.8333340000000007    0.6666659999999993    0.6398787726831945
  0.0000000000000000    0.0000000000000000    0.4432577474539330
  0.0000000000000000    0.5000000000000000    0.4432577474539330
  0.5000000000000000    0.0000000000000000    0.4432577474539330
  0.5000000000000000    0.5000000000000000    0.4432577474539330
  0.0000000000000000    0.0000000000000000    0.5567422525459885
  0.0000000000000000    0.5000000000000000    0.5567422525459885
  0.5000000000000000    0.0000000000000000    0.5567422525459885
  0.5000000000000000    0.5000000000000000    0.5567422525459885
  0.3333340000000007    0.1666659999999993    0.5000000000000000
  0.3333340000000007    0.6666659999999993    0.5000000000000000
  0.8333340000000007    0.1666659999999993    0.5000000000000000
  0.8333340000000007    0.6666659999999993    0.5000000000000000
  0.1666659999999993    0.3333340000000007    0.5000000000000000
  0.1666659999999993    0.8333340000000007    0.5000000000000000
  0.6666659999999993    0.3333340000000007    0.5000000000000000
  0.6666659999999993    0.8333340000000007    0.5000000000000000


Na8 Mg8 B8 (POSCAR)
   1.00000000000000
```

6.3063046570740191	0.0000001671392878	0.0000000000000000
-3.1531460584981676	5.4614206885561991	0.0000000000000000
0.0000000000000000	0.0000000000000000	33.0505128388136953

Na   Mg   B
 8   8   8
Direct

0.3333340000000007	0.1666659999999993	0.6364322576283322
0.3333340000000007	0.6666659999999993	0.6364322576283322
0.8333340000000007	0.1666659999999993	0.6364322576283322
0.8333340000000007	0.6666659999999993	0.6364322576283322
0.3333340000000007	0.1666659999999993	0.3635677423716747
0.3333340000000007	0.6666659999999993	0.3635677423716747
0.8333340000000007	0.1666659999999993	0.3635677423716747
0.8333340000000007	0.6666659999999993	0.3635677423716747
0.0000000000000000	0.0000000000000000	0.4499417586157406
0.0000000000000000	0.5000000000000000	0.4499417586157406
0.5000000000000000	0.0000000000000000	0.4499417586157406
0.5000000000000000	0.5000000000000000	0.4499417586157406
0.0000000000000000	0.0000000000000000	0.5500582413842665
0.0000000000000000	0.5000000000000000	0.5500582413842665
0.5000000000000000	0.0000000000000000	0.5500582413842665
0.5000000000000000	0.5000000000000000	0.5500582413842665
0.3333340000000007	0.1666659999999993	0.5000000000000000
0.3333340000000007	0.6666659999999993	0.5000000000000000
0.8333340000000007	0.1666659999999993	0.5000000000000000
0.8333340000000007	0.6666659999999993	0.5000000000000000
0.1666659999999993	0.3333340000000007	0.5000000000000000
0.1666659999999993	0.8333340000000007	0.5000000000000000

0.6666659999999993   0.3333340000000007   0.5000000000000000

0.6666659999999993   0.8333340000000007   0.5000000000000000

Na8 Mg8 B8 (CONTCAR)

1.00000000000000

    6.3063037611449602   0.0000001671382117   0.0000000000000000

   -3.1531456105354403   5.4614199126590988   0.0000000000000000

    0.0000000000000000   0.0000000000000000   33.0505128388136953

   Na   Mg   B

    8   8   8

Direct

  0.3333340000000007   0.1666659999999993   0.6364323061838356

  0.3333340000000007   0.6666659999999993   0.6364323061838356

  0.8333340000000007   0.1666659999999993   0.6364323061838356

  0.8333340000000007   0.6666659999999993   0.6364323061838356

  0.3333340000000007   0.1666659999999993   0.3635676938161716

  0.3333340000000007   0.6666659999999993   0.3635676938161716

  0.8333340000000007   0.1666659999999993   0.3635676938161716

  0.8333340000000007   0.6666659999999993   0.3635676938161716

 -0.0000000000000000   0.0000000000000000   0.4499418214084155

 -0.0000000000000000   0.5000000000000000   0.4499418214084155

  0.5000000000000000   0.0000000000000000   0.4499418214084155

  0.5000000000000000   0.5000000000000000   0.4499418214084155

 -0.0000000000000000   0.0000000000000000   0.5500581785915916

 -0.0000000000000000   0.5000000000000000   0.5500581785915916

  0.5000000000000000   0.0000000000000000   0.5500581785915916

  0.5000000000000000   0.5000000000000000   0.5500581785915916

  0.3333340000000007   0.1666659999999993   0.5000000000000000

```
0.3333340000000007    0.6666659999999993    0.5000000000000000
0.8333340000000007    0.1666659999999993    0.5000000000000000
0.8333340000000007    0.6666659999999993    0.5000000000000000
0.1666659999999993    0.3333340000000007    0.5000000000000000
0.1666659999999993    0.8333340000000007    0.5000000000000000
0.6666659999999993    0.3333340000000007    0.5000000000000000
0.6666659999999993    0.8333340000000007    0.5000000000000000


Na8 Ca8 B8 (POSCAR)
  1.00000000000000
     6.7351088810539492    0.0000001525283601    0.0000000000000000

    -3.3675407535176314    5.8327805040108354    0.0000000000000000
     0.0000000000000000    0.0000000000000000    33.3047817894384721

   Na   Ca    B
    8    8    8
Direct
  0.3333340000000007    0.1666659999999993    0.3471600943872775
  0.3333340000000007    0.6666659999999993    0.3471600943872775
  0.8333340000000007    0.1666659999999993    0.3471600943872775
  0.8333340000000007    0.6666659999999993    0.3471600943872775
  0.1666659999999993    0.3333340000000007    0.6528399056127319
  0.1666659999999993    0.8333340000000007    0.6528399056127319
  0.6666659999999993    0.3333340000000007    0.6528399056127319
  0.6666659999999993    0.8333340000000007    0.6528399056127319
 -0.0000000000000000   -0.0000000000000000    0.4440844743546665
 -0.0000000000000000    0.5000000000000000    0.4440844743546665
  0.5000000000000000   -0.0000000000000000    0.4440844743546665
  0.5000000000000000    0.5000000000000000    0.4440844743546665
```

```
-0.0000000000000000 -0.0000000000000000   0.5559155256453013
-0.0000000000000000   0.5000000000000000   0.5559155256453013
 0.5000000000000000 -0.0000000000000000   0.5559155256453013
 0.5000000000000000   0.5000000000000000   0.5559155256453013
 0.3333340000000007   0.1666659999999993   0.4999686647572359
 0.3333340000000007   0.6666659999999993   0.4999686647572359
 0.8333340000000007   0.1666659999999993   0.4999686647572359
 0.8333340000000007   0.6666659999999993   0.4999686647572359
 0.1666659999999993   0.3333340000000007   0.5000313352427621
 0.1666659999999993   0.8333340000000007   0.5000313352427621
 0.6666659999999993   0.3333340000000007   0.5000313352427621
 0.6666659999999993   0.8333340000000007   0.5000313352427621
```

Na8 Ca8 B8 (CONTCAR)
```
   1.00000000000000
      6.7349287007819942      0.0000001512663633      0.0000000000000000

     -3.3674506648372144      5.8326244629916104      0.0000000000000000
      0.0000000000000000      0.0000000000000000     33.3047817894384721
```

```
  Na    Ca     B
   8     8     8
```
Direct
```
 0.3333340000000007   0.1666659999999993   0.6529440144508669
 0.3333340000000007   0.6666659999999993   0.6529440144508669
 0.8333340000000007   0.1666659999999993   0.6529440144508669
 0.8333340000000007   0.6666659999999993   0.6529440144508669
 0.3333340000000007   0.1666659999999993   0.3470559855491331
 0.3333340000000007   0.6666659999999993   0.3470559855491331
 0.8333340000000007   0.1666659999999993   0.3470559855491331
```

0.8333340000000007	0.6666659999999993	0.3470559855491331
0.0000000000000000	0.0000000000000000	0.4440751606375883
0.0000000000000000	0.5000000000000000	0.4440751606375883
0.5000000000000000	0.0000000000000000	0.4440751606375883
0.5000000000000000	0.5000000000000000	0.4440751606375883
0.0000000000000000	0.0000000000000000	0.5559248393623832
0.0000000000000000	0.5000000000000000	0.5559248393623832
0.5000000000000000	0.0000000000000000	0.5559248393623832
0.5000000000000000	0.5000000000000000	0.5559248393623832
0.3333340000000007	0.1666659999999993	0.5000000000000000
0.3333340000000007	0.6666659999999993	0.5000000000000000
0.8333340000000007	0.1666659999999993	0.5000000000000000
0.8333340000000007	0.6666659999999993	0.5000000000000000
0.1666659999999993	0.3333340000000007	0.5000000000000000
0.1666659999999993	0.8333340000000007	0.5000000000000000
0.6666659999999993	0.3333340000000007	0.5000000000000000
0.6666659999999993	0.8333340000000007	0.5000000000000000

References

[1] Q. He, Z. Li, W. Xiao, C. Zhang, Y. Zhao, Computational investigation of 2D 3d/4d hexagonal transition metal borides for metal-ion batteries, Electrochimica Acta 384 (2021) 138404. https://doi.org/10.1016/j.electacta.2021.138404.

[2] T. Bo, P.-F. Liu, J. Xu, J. Zhang, Y. Chen, O. Eriksson, F. Wang, B.-T. Wang, Hexagonal Ti_2B_2 monolayer: a promising anode material offering high rate capability for Li-ion and Na-ion batteries, Phys. Chem. Chem. Phys. 20 (2018) 22168–22178. https://doi.org/10.1039/C8CP03362E.

[3] G. Yuan, T. Bo, X. Qi, P.-F. Liu, Z. Huang, B.-T. Wang, Monolayer Zr_2B_2: a promising two-dimensional anode material for Li-ion batteries, Appl. Surf. Sci. 480 (2019) 448–453. https://doi.org/10.1016/j.apsusc.2019.02.222.

[4] S. Gao, J. Hao, X. Zhang, L. Li, C. Zhang, L. Wu, X. Ma, P. Lu, G. Liu, Two dimension transition metal boride Y_2B_2 as a promising anode in Li-ion and

Na-ion batteries, Comput. Mater. Sci. 200 (2021) 110776. https://doi.org/10.1016/j.commatsci.2021.110776.

[5] M. Liang, L. Zhi, Graphene-based electrode materials for rechargeable lithium batteries, J. Mater. Chem. 19 (2009) 5871–5878. https://doi.org/10.1039/B901551E.

[6] Z. Guo, J. Zhou, Z. Sun, New two-dimensional transition metal borides for Li ion batteries and electrocatalysis, J. Mater. Chem. A 5 (2017) 23530–23535. https://doi.org/10.1039/C7TA08665B.

[7] D. Er, J. Li, M. Naguib, Y. Gogotsi, V.B. Shenoy, Ti_3C_2 MXene as a high capacity electrode material for metal (Li, Na, K, Ca) ion batteries, ACS Appl. Mater. Interfaces 6 (2014) 11173–11179. https://doi.org/10.1021/am501144q.

[8] M. Endo, C. Kim, K. Nishimura, T. Fujino, K. Miyashita, Recent development of carbon materials for Li ion batteries, Carbon 38 (2000) 183–197. https://doi.org/10.1016/S0008-6223(99)00141-4.

[9] Y. Yu, Z. Guo, Q. Peng, J. Zhou, Z. Sun, Novel two-dimensional molybdenum carbides as high capacity anodes for lithium/sodium-ion batteries, J. Mater. Chem. A 7 (2019) 12145–12153. https://doi.org/10.1039/C9TA02650A.

[10] M. Mortazavi, C. Wang, J. Deng, V.B. Shenoy, N.V. Medhekar, Ab initio characterization of layered MoS_2 as anode for sodium-ion batteries, J. Power Sources 268 (2014) 279–286. https://doi.org/10.1016/j.jpowsour.2014.06.049.

[11] A. Kumar, P. Parida, Unveiling the potential of a BCN-biphenylene monolayer as a high-performance anode material for alkali metal ion batteries: a first-principles study, Nanoscale 16 (2024) 13131–13147. https://doi.org/10.1039/D4NR01386G.